THE JOURNAL OF PHYSICAL CHEMISTRY C

Article

Cite This: J. Phys. Chem. C 2018, 122, 18501−18509

pubs.acs.org/JPCC

Screening Surface Structure of MXenes by High-Throughput Computation and Vibrational Spectroscopic Confirmation

Tao Hu,[†,‡] Minmin Hu,[†,§] Bo Gao,[∥] Wu Li,*[,⊥] and Xiaohui Wang*[,†]

[†]Shenyang National Laboratory for Materials Science, Institute of Metal Research, Chinese Academy of Sciences, 72 Wenhua Road, Shenyang 110016, China

[‡]Institute of Materials Science and Devices, Suzhou University of Science and Technology, Suzhou 215009, China

[§]School of Materials Science and Engineering, University of Science and Technology of China, Shenyang 110016, China

[∥]Center for Materials Research by Information Integration (CMI2), National Institute for Materials Science (NIMS), 1-1 Namiki, Tsukuba, Ibaraki 305-0044, Japan

[⊥]Institute for Advanced Study, Shenzhen University, Shenzhen 518060, China

Supporting Information

ABSTRACT: Functionalized MXenes hold promises in a variety of applications in which the dispensable functional groups are mixed. The functionalization is spontaneously realized through competitive adsorption of active species on the MX matrix during the acid etching process of MAX phases. Nevertheless, the knowledge of proportion and distribution of functional groups on MXenes, i.e., surface structures, is still limited. By high-throughput computation screening, ground-state stable structures of four kinds of typical MXenes—Ti_2CT_x, $Ti_3C_2T_x$, Nb_2CT_x, and $Nb_4C_3T_x$ (T = O, F, and OH)—with mixed functional group compositions are figured out for the first time. The multicomponent functional group patterns definitely demonstrate an obvious feature of spatial mixing at a given component. However, the heterogeneous structure has a near linear dependence on the functional group components in terms of free energy. Most functionalized MXenes are dynamically stable except for Nb_2CF_2 and $Nb_2C(OH)_2$ due to their competing displacive counterparts. Last but not least, Raman spectra of the four kinds of MXenes confirm the predicted stable surface structures of MXenes. This study provides a clear fundamental basis for understanding the surface structures of MXenes.

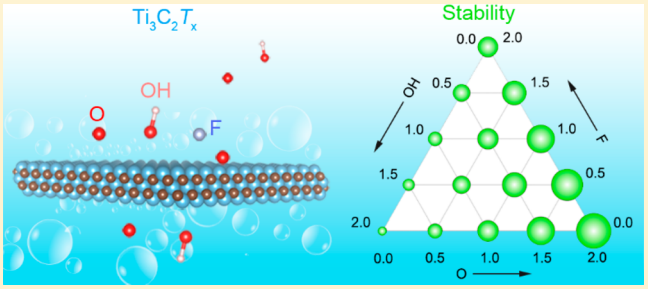

INTRODUCTION

Competitive adsorption is ubiquitous in chemical separation, electrochemistry, and heterogeneous catalysis.[1−3] The competitive factors include but are not limited to the aspects of adsorption species,[4] adsorption sites,[5] and adsorbate distribution patterns.[2] Clarifying the competing relationship between the factors plays key roles in determining the processes that actually happen at the surface in a complex aqueous environment or a gaseous atmosphere and rationally designing desired structures with preferred properties. Nevertheless, reliable prediction regarding stable surface structures and quantitative understanding of such a critical competitive mechanism is long-lacking due to its complexity and the lack of available methods. Fortunately, the recent development of accurate surface structure prediction methodology and high-throughput computation altogether have made it possible so far.

MXenes represent a burgeoning large family of two-dimensional (2-D) materials of transition metal carbides/carbonitrides. They are usually obtained by selectively etching off certain atomic layers A from layered precursors such as MAX phases and analogues.[6,7] Being synthesized in aqueous solutions, MXenes are featured by competitive adsorption among functional groups like O, F, and OH on the chemically active surface of MX slabs.[8,9] Though terminations have shown vital roles in many applications of MXenes,[9−18] controlling terminations toward desired properties remains challenging. A deep understanding of the termination process is a prerequisite for rationally tailoring surface structures of MXenes. However, the knowledge about the composition and distributions of terminations is very limited.[8,19−21] Experimentally, the terminations show a coexisting feature, but their proportions considerably vary from one report to another.[22−25] Most theoretical works only tackle the situation of homogeneous termination by O, F, and OH groups or artificially built half−half terminated models, leaving termination-mixed cases unresolved.[20,26] Motivated by the urgency of clarifying the termination composition and distribution, this work is

Received: May 9, 2018
Revised: July 22, 2018
Published: July 23, 2018

DOI: 10.1021/acs.jpcc.8b04427
J. Phys. Chem. C 2018, 122, 18501−18509

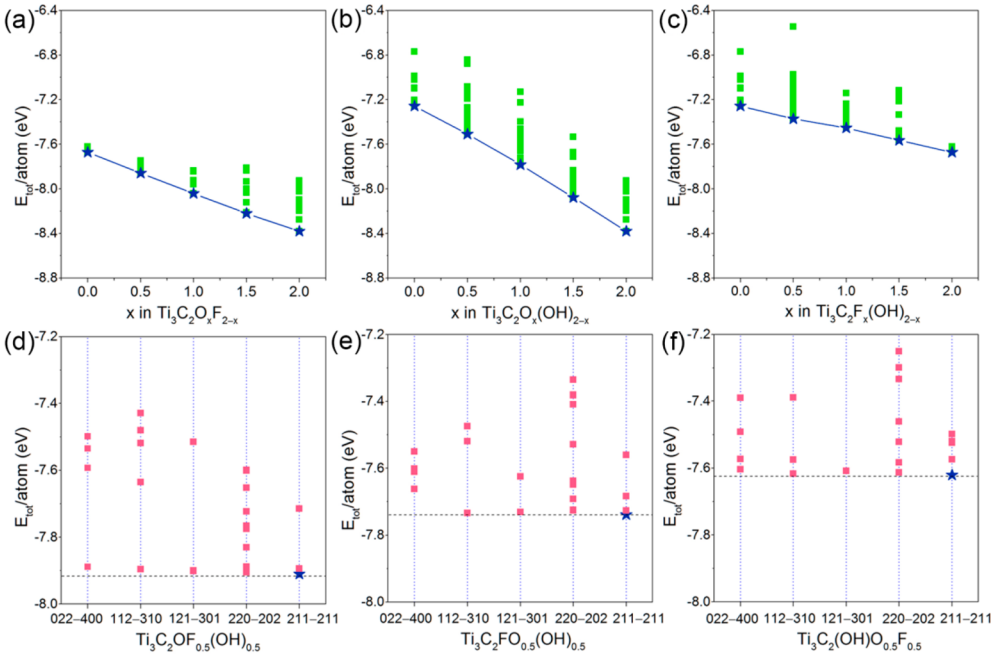

Figure 1. Energetic distributions of 450 structures for functionalized $Ti_3C_2T_x$ MXenes. (a) $Ti_3C_2O_xF_{2-x}$, (b) $Ti_3C_2O_x(OH)_{2-x}$, (c) $Ti_3C_2F_x(OH)_{2-x}$, (d) $Ti_3C_2OF_{0.5}(OH)_{0.5}$, (e) $Ti_3C_2FO_{0.5}(OH)_{0.5}$, and (f) $Ti_3C_2(OH)O_{0.5}F_{0.5}$ MXenes. The blue line forms the ground-state hull joining the lowest free energy structures across the compositions. The digitals (*ijk*–*lmn*) in tick labels of (d–f) represent the numbers of −O, −F, and −OH are *i*, *j*, and *k* on one surface of a single layer and *l*, *m*, and *n* on the other surface, respectively. Note that many of the searched structures have similar free energies so that some points are hidden by others.

dedicated to investigating the termination-mixed patterns and their stability. High-throughput computation, which has demonstrated its superior power in effectively searching for stable ordering MXene alloys recently,[27] provides a powerful tool to screen the stable MXene surface structures.

In this work, we provide, for the first time, the systematical investigation of ground-state structures and relative stability of MXenes with unary, binary, and ternary termination components (O, F, and OH) by high-throughput computation. Surface structures of four typical MXenes—Ti_2CT_x, $Ti_3C_2T_x$, Nb_2CT_x, and $Nb_4C_3T_x$—with various *M* elements and layer thicknesses are screened comprehensively. Besides, data mining of the intensive calculations allows us to clarify the contributions of critical factors, including adsorbate species, adsorption sites, in-plane patterns, and surface–surface interactions to the thermodynamic stability. Last but not least, the theoretically predicted stable MXenes were further confirmed by micro-Raman spectroscopy. This study provides a clear fundamental basis for understanding the surface structures of MXenes.

METHODS

Ab initio density functional theory (DFT) plus particle swarm optimization algorithm as implemented in Crystal structure AnaLysis by Particle Swarm Optimization (CALYPSO) code[28,29] was employed in this study to guarantee the accuracy. In this method, we generated the initial structure by fixing the substrate while randomly dispersed adsorbates on both equivalent surfaces of the substrate. To reduce the constraints imposed by periodicity, a 2 × 2 × 1 supercell was used as substrate (12 atoms/cell for Ti_2C and Nb_2C, 20 atoms/cell for Ti_3C_2, and 28 atoms/cell for Nb_4C_3). A sample size of 30 structures per one generation was large enough, as the most favorable adsorption configurations were figured out in the first loop.

All DFT computations were performed by using the plane-wave technique as implemented in the Vienna ab initio simulation package (VASP).[30] The electron–ion interaction was described by projector augmented wave pseudopotentials.[31] The exchange correlation energy was described by the generalized gradient approximation (GGA) in the scheme proposed by Perdew–Burke–Ernzerhof (PBE).[32] A 500 eV cutoff energy was used for the plane-wave basis set. A vacuum region of about 15 Å was intercalated between the adjacent MXene layers to avoid interlayer interactions. The Monkhorst–Pack scheme with 14 × 14 × 1 *k* point meshes was used for the integration in the irreducible Brillouin zone so that the individual spacing was less than 0.05 $Å^{-1}$. The convergence threshold for energy was chosen as 1.0×10^{-6} eV/atom, and the structures were relaxed until the maximum force exerted on the atoms became less than 0.001 eV/Å. Because no spin polarization effect was reported in terminated Ti- and Nb-containing MXenes according to earlier studies,[20,33−37] magnetism was not considered in the study of the thermodynamics and vibrational properties of ground-state structures of the select MXenes. Benchmark calculations (see Figures S1 and S2) indicate that the results obtained by the present PBE potentials are reliable, and the dipole does not contribute much to total energy of MXenes. Phonon spectra were calculated using the PHONOPY package with the finite displacement method.[38] The force constant matrix was constructed by slight displacement of atoms in a 6 × 6 × 1 supercell.

The lamellae for the micro-Raman spectroscopy investigation were synthesized by exfoliating their corresponding porous MAX phases. The MAX phases were prepared by the method reported previously.[39−42] $Ti_3C_2T_x$, Nb_2CT_x, and

DOI: 10.1021/acs.jpcc.8b04427
J. Phys. Chem. C 2018, 122, 18501−18509

$Nb_4C_3T_x$ were obtained by exfoliating porous Ti_3AlC_2 (1 g), Nb_2AlC (1 g), and Nb_4AlC_3 (1 g) in 10 mL of 40 wt % HF for 24 h, 3 months, and 8 months at room temperature, respectively. Ti_2CT_x was synthesized by exfoliating porous Ti_2AlC (1.08 g) in 40 mL of 7.5 mol/L hydrochloric acid (HCl) with NH_4F addition (1.50 g) for 8 days at room temperature. After that, the resulting sediments were washed several times using deionized water, followed by immersion in deionized water for 1 day and subsequent vacuum filtration. The collected powders were dried in an oven at 60 °C for 10 h before Raman measurement. The unpolarized Raman spectra of the exfoliated lamellae were collected on a LabRAM HR800 (Jobin Yvon, France) equipped with an air-cooled CCD array detector in the backscattering configuration. For the Raman measurements, a long-working-distance 50× objective with numerical aperture of 0.50 was used. A He−Ne laser (632.8 nm) was used, and the laser power was kept below 4 mW on the sample surface to avoid laser-induced heating. Two kinds of gratings (600 lines/mm for $Ti_3C_2T_x$ and Ti_2CT_x and 1800 lines/mm for Nb_2CT_x and $Nb_4C_3T_x$) were used for single Raman spectrum measurement to achieve high spectral resolution.

RESULTS AND DISCUSSION

For the sake of high-throughput computation screening, it is constructive to choose a suitable descriptor for the thermodynamic stability of terminated MXenes first. In a system with strong chemical adsorption,[19] the 2-D substrate may change dramatically upon termination; thus, the classical "binding energy" of terminations on the matrix actually contains the strain energy of the distorted substrate. Enthalpy, the stability descriptor usually used in bulk systems, is also unsuitable due to the vacuum-containing volume for 2-D models. In contrast, the free energy is a universal stability descriptor regardless of substrate distortion or volume. Thus, in this work, free energy per atom was used to evaluate stability among different MXene species. The free energy per atom ($E_{tot/atom}$) is defined as follows:

$$E_{tot/atom} = \frac{E_{tot} - \sum_N E_{atom\_i}}{N} \quad (1)$$

Here N, E_{tot}, and E_{atom_i} represent the number of atoms in a unit, the total energy of MXene, and single atom_i, respectively. Enlightened by ternary phase diagram, we designed the components and proportions of termination based on the "ternary phase diagram" of O, F, and OH. This sophisticated search strategy had been proved to be efficient to pinpoint the most favorable termination configurations without missing any target structures as shown in the following passage. Over 450 different structures were checked for each kind of MXene to elucidate the energetically favorable distribution patterns of single/multicomponent terminations. Figure 1a−c presents the free energy evolution upon functional group components in unary and binary functionalized $Ti_3C_2T_x$ MXenes, while Figure 1d−f shows the energy distribution of ternary-functionalized ones. Interestingly, the convex hulls presented in Figure 1a−c indicate that the free energy shows a near linear dependence on the termination proportions. This relationship is also found in other three kinds of MXenes: Ti_2CT_x, Nb_2CT_x, and $Nb_4C_3T_x$, as presented in Figures S3−S5 for brevity.

One unanticipated finding is the dehydrogenation phenomenon in OH-containing MXenes during the structure search process. That is, OH groups became O groups and H_2 gas (see Figure S6). On the basis of this phenomenon, we compared the free energies of $M_{n+1}X_n(OH)_2$ and $M_{n+1}X_nO_2 + H_2$ (M = Ti and Nb, n = 1 and 2 for Ti, n = 1 and 3 for Nb). As shown in Table 1, the free energy of $M_{n+1}C_nO_2 + H_2$ is lower than those of $M_{n+1}C_n(OH)_2$. The results presented here indicate that high concentration OH-terminated MXenes tend to form O-terminated MXenes and H_2 gas. This is in excellent agreement with earlier work[19,37,43−45] that O is the most stable termination. Furthermore, $Nb_2C(OH)_2$ with the largest $|\Delta E/OH|$ has the largest tendency toward Nb_2CO_2, indicating the instability of $Nb_2C(OH)_2$ as will be described below, in agreement with the most recent experimental observation.[46]

Table 1. Energy Differences of $M_{n+1}X_n(OH)_2$ and $M_{n+1}X_nO_2$ + H_2 per OH Group[a]

formula	ΔE/OH (eV)
$Ti_2C(OH)_2 \rightarrow Ti_2CO_2 + H_2$	−0.08
$Ti_3C_2(OH)_2 \rightarrow Ti_3C_2O_2 + H_2$	−0.02
$Nb_2C(OH)_2 \rightarrow Nb_2CO_2 + H_2$	−0.43
$Nb_4C_3(OH)_2 \rightarrow Nb_4C_3O_2 + H_2$	−0.16

[a] $\Delta E = E(M_{n+1}X_nO_2 + H_2) - E(M_{n+1}X_n(OH)_2)$.

Interestingly, during the structure search of F- and OH-containing Nb_2CT_x MXenes, two new phases (*Cm* Nb_2CF_2 and *P*3*m*1 $Nb_2C(OH)_2$) were observed. Unlike the $P\bar{3}m1$ phases[34] reported earlier, the newly found *Cm* Nb_2CF_2 and *P*3*m*1 $Nb_2C(OH)_2$ have some drastic atomic displacements compared with their counterparts, and are named displacive phases hereafter, as shown in Figure S7. The displacive phases *Cm* Nb_2CF_2 and *P*3*m*1 $Nb_2C(OH)_2$ with distorted Nb-centered octahedrons are energetically more stable compared with the $P\bar{3}m1$ Nb_2CF_2 and $Nb_2C(OH)_2$. Because of the dynamically instability of both displacive and nondisplacive Nb_2CF_2 and $Nb_2C(OH)_2$ as will be discussed in the following section, Nb_2CT_x is excluded when we refer to multicomponent MXenes hereafter unless specified otherwise.

For a given chemical formula MXene, the termination contributes to the free energy of the system through three interactions: first, the interaction between adsorbates and substrate which mainly concerns adsorption sites; second, the adsorbate−adsorbate interaction which involves interactions between terminations and their neighbors adsorbed on the same surface forming an in-plane distribution pattern; third, the surface−surface interaction, viz., the correlation between one in-plane distribution pattern and that on the other side of a single MXene layer. To probe the roles of the three kinds of interactions play in the system, we examined the energy fluctuations of each kind of interactions as presented in Figure 2. Here the energy fluctuation is defined as the energy difference between the most favorable configurations and their competing counterparts. For example, the energy fluctuation of adsorption sites is the energy difference between the two most favorable competing adsorption configurations (for $Ti_3C_2T_x$, face-centered cubic (FCC) and hexagonal close packing (HCP) sites are competitive, see Figure 3a).[47] Through careful data mining, it is found that the contributions of the three interactions to thermodynamics follow the order adsorption site > in-plane distribution pattern > surface−surface correlation, as shown in Figure 2.

DOI: 10.1021/acs.jpcc.8b04427
J. Phys. Chem. C 2018, 122, 18501−18509

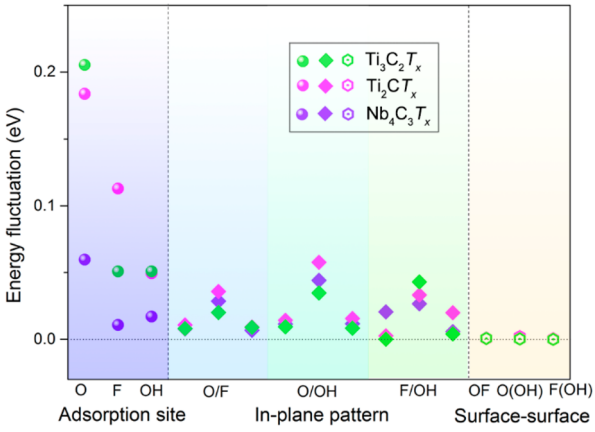

Figure 2. Energy fluctuation of three kinds of interactions in functionalized $Ti_3C_2T_x$, Ti_2CT_x, and $Nb_4C_3T_x$ MXenes. The contribution to the free energy follows the order adsorbate−substrate interaction > adsorbate−adsorbate interaction > surface−surface correlation. The three values from left to right for each of these categories in the in-plane pattern correspond to $T1/T2$ = 0.5, 1, and 2.

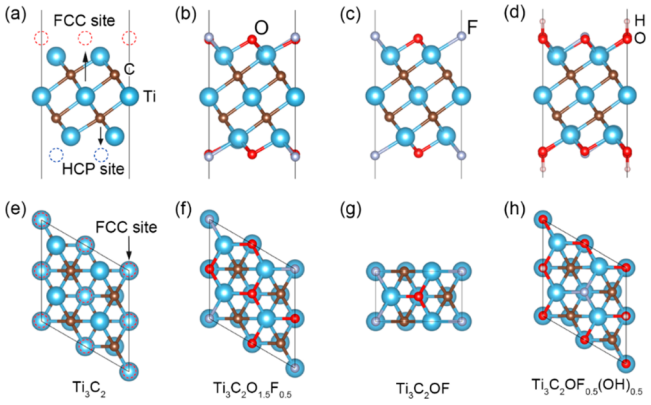

Figure 3. Most stable configurations of O-containing $Ti_3C_2T_x$ MXenes. (a−d) Side view and (e−h) top view. All terminations locate at the FCC sites.

As shown above, adsorption sites significantly affect the thermodynamics of the system. Thus, determining the adsorption sites is crucial in figuring out the distribution patterns. A careful survey of recent literature indicates the necessity of a more systematical and thorough consideration in determining adsorption sites of MXenes.[48,49] The traditional trial-and-error method of comparing high-symmetry adsorption sites seems crude and inefficient. In contrast, the global surface structure search method implanted in CALYPSO makes it elegant and efficient. It accurately figured out the distinct adsorption sites in different MXenes though the only input information is the structure of substrate and the adsorption species and their proportions. For Ti_2CT_x, $Ti_3C_2T_x$, Nb_2CT_x, and $Nb_4C_3O_2$, FCC sites are found to be the most favorable adsorption sites.[34,49] However, for $Nb_4C_3F_2$, and $Nb_4C_3(OH)_2$, HCP sites are the most favorable. Instead of forming octahedrons, the surfaces Nb in $Nb_4C_3F_2$ and $Nb_4C_3(OH)_2$ change their coordination and form Nb-centered triangle prisms. This is presumably due to the more extended 4d states of the transition metal Nb.[50] The distinct chemisorption behaviors between Nb_2C and Nb_4C_3 demonstrate that the layer thickness is an important parameter in tailoring the properties of MXene.[44]

Though adsorbate−adsorbate and surface−surface interactions are much weaker than the robust adsorbate−substrate interaction, it is possible to work out the regular termination-mixed pattern based on the accurate ab initio calculation. The surface−surface correlation is the weakest among the three kinds of interactions due to its long-range nature and screening effect. Figure 3 illustrates the most favorable mixed distribution patterns of O-containing $Ti_3C_2T_x$. FCC sites are the energetically most favorable adsorption sites in unary, binary, or ternary functionalized $Ti_3C_2T_x$ MXenes. The same termination species on the same surface exhibit a repulsive nature, thus maximizing the distance between them (Figure S8). Besides, the identical termination tends to chemisorb averagely on both surfaces rather than on the same surface. The simultaneously atomically dispersed functional group distribution is highly desirable for high-efficiency catalysis like single-atom catalysis.[51]

The relative stability of the termination-mixed MXenes is a concerning issue because it holds the promises for understanding the experimental results and guiding the modification of the MXene surface. Here, the thermodynamic stability of different terminated MXenes is presented by the ternary bubble plot within the framework of the O, F, and OH "termination ternary diagram" (see Figure 4). The formula used for bubble size is

$$R_B = \frac{E - E_{min}}{E_{max} - E_{min}} \times (R_{max} - R_{min}) + R_{min} \quad (2)$$

where R_B is the bubble radius, E the absolute value of free energy, E_{min} the minimum absolute value of free energy, E_{max} the maximum absolute value of free energy, R_{min} the minimum radius, and R_{max} the maximum radius. Thus, the bubble size (Table S1) represents the thermodynamic stability of the MXenes at different terminated compositions. The bubble plot gives a straightforward and intuitionistic comparison of relative stability. From an aspect of statistics, the size of the bubble represents the possibility of forming such a terminated structure.

The thermodynamic stabilities of terminated MXenes shown in Figure 4 share some similar trends: in all three kinds of MXenes, the stability increases from OH to F to O. This is consistent with the near linear trend indicated by convex hulls presented in Figure 1 and Figures S3−S5. The OH-terminated MXenes are the least stable among the MXenes considered, agreeing with the dehydrogenation observed during the global search process. The MXenes tend to form O-terminated MXenes at the ideal O-rich environment because O-terminated $Ti_3C_2O_2$, Ti_2CO_2, and $Nb_4C_3O_2$ are the most energetically favorable. Besides, according to recent study, O-predominant MXene surface groups enable MXene a promising high-performance electrochemical capacitor standing up to RuO_2.[12,52] However, under ambient synthesis conditions, terminations show a coexisting feature in experimental samples. It must be mentioned that a shortcoming of the present investigation is the lack of treatment of solvation effect. Extra efforts have to be made to figure out the influence of kinetics process, temperature, pH, electropotentials, partial pressure, and other experimental factors, but it is beyond the scope of this study.

DOI: 10.1021/acs.jpcc.8b04427
J. Phys. Chem. C 2018, 122, 18501−18509

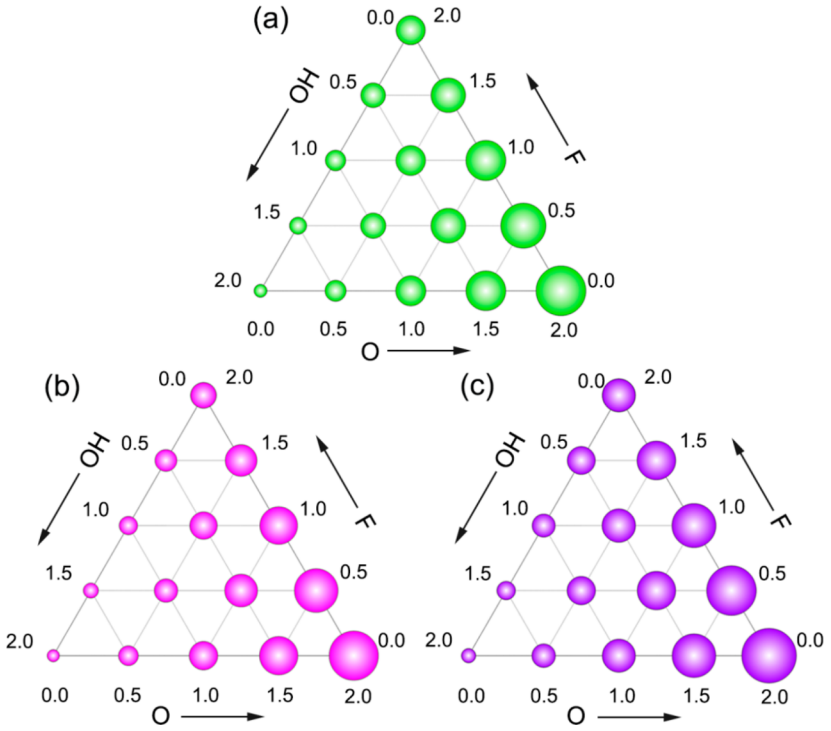

Figure 4. Relative stability bubble plots for (a) $Ti_3C_2O_xF_y(OH)_z$, (b) $Ti_2CO_xF_y(OH)_z$, and (c) $Nb_4C_3O_xF_y(OH)_z$. The bubble size represents the relative stability of a certain MXene.

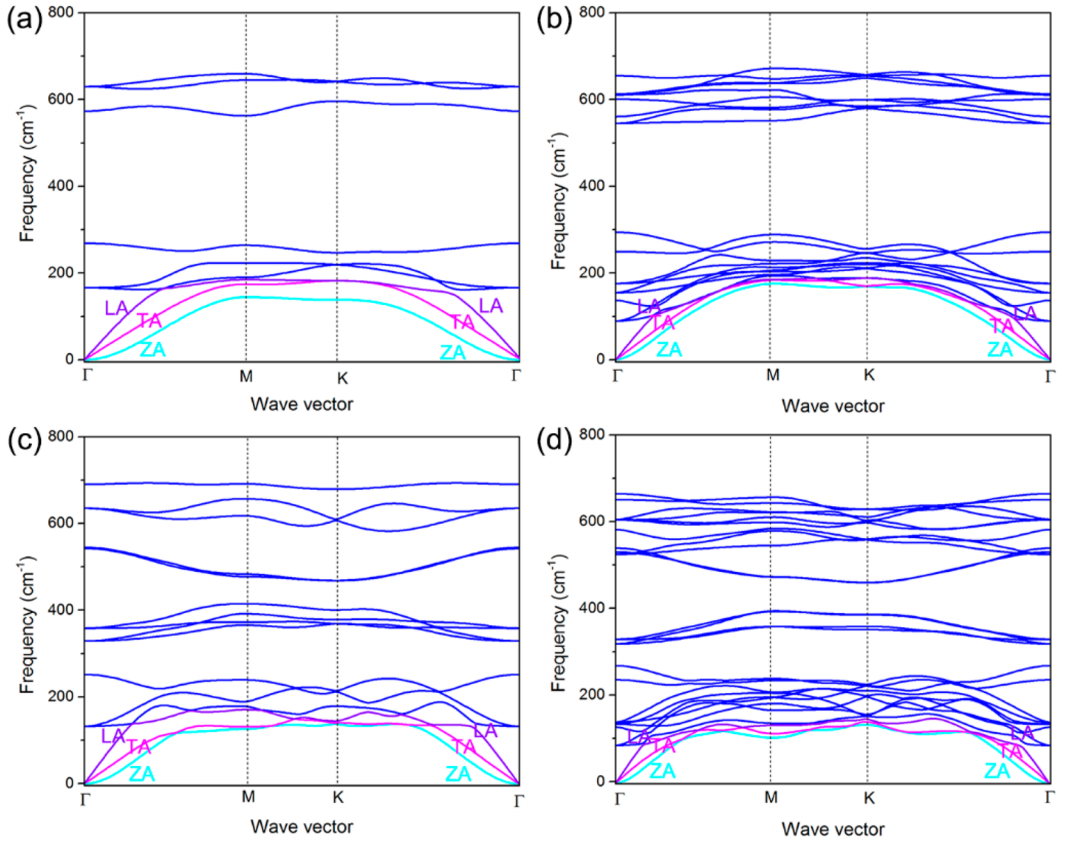

Figure 5. Phonon dispersions of (a) Nb_2C, (b) Nb_4C_3, (c) Nb_2CO_2, and (d) $Nb_4C_3O_2$ MXene. The cyan, magenta, and violet lines represent the ZA branch, the transverse acoustic (TA), and the longitude acoustic (LA) phonon, respectively.

The ground-state structures of MXenes at each given chemical component have been determined hitherto. Generally speaking, the ground-state structures are the most stable species from the perspective of thermodynamics. One more

DOI: 10.1021/acs.jpcc.8b04427
J. Phys. Chem. C 2018, 122, 18501−18509

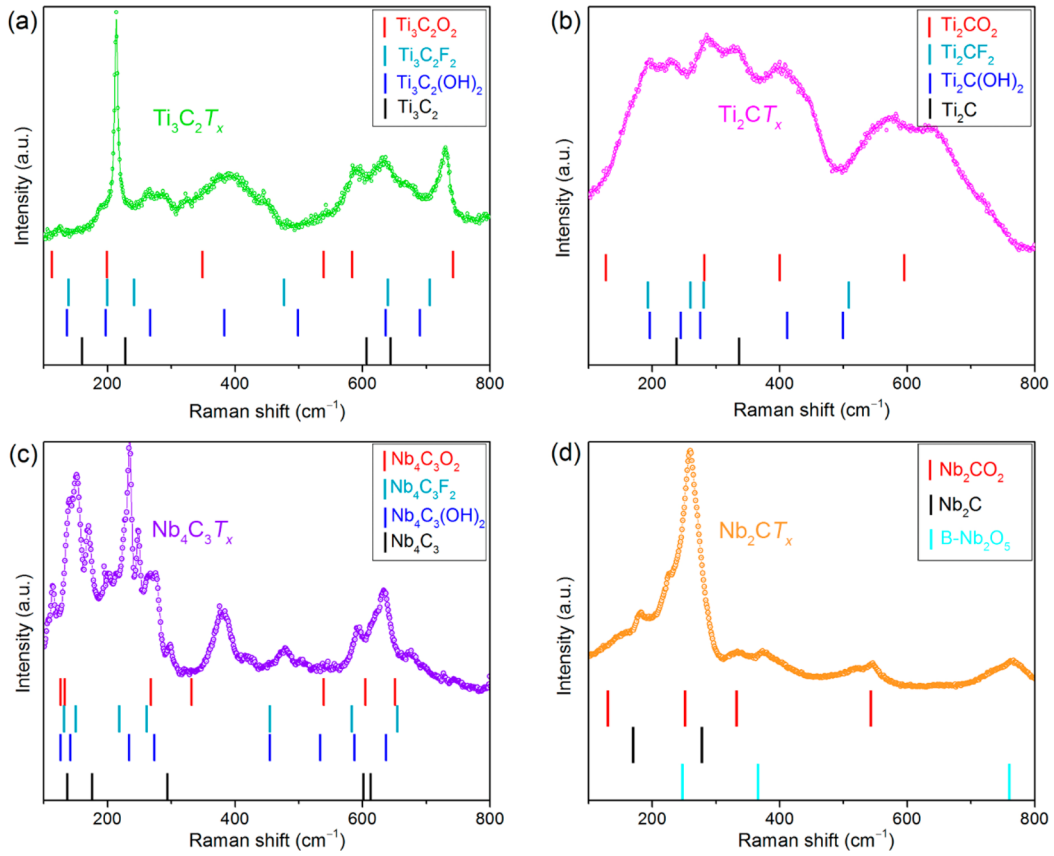

Figure 6. Raman spectra of synthesized (a) $Ti_3C_2T_x$, (b) Ti_2CT_x, (c) $Nb_4C_3T_x$, and (d) Nb_2CT_x lamella. Calculated Raman-active frequencies are also included, and they roughly match the bands in the spectra. Note that Raman shifts of Nb_2C and Nb_2CO_2 can explain most peaks in the Raman spectrum of Nb_2CT_x.

step needed is to check the dynamical stability which is governed by the interatomic force constants (IFC). The transition metal carbide slab matrix shows good dynamical stability due to the strong M−C bonds (Figure 5a,b). Thus, the key of dynamical stability of terminated MXenes lies at the interaction between terminations and the matrix. Based on this knowledge, the phonon dispersions of homogeneously terminated MXenes are used to evaluate the compatibility of termination and matrix in these MXenes. The dynamical stability of homogeneously terminated MXene indicates that the force constant between T and matrix is favorable and T can form locally dynamically stable structures with the matrix, and vice versa. Through a reformulation of IFC in terms of internal coordinates, physically sound phonon dispersion are obtained, as evidenced by Figure 5 that out-of-plane flexural modes (ZA) of bare and O-terminated Nb_2C and Nb_4C_3 MXenes are all quadratic due to the 2-D nature.[53] Phonon dispersions of both Ti_2CT_2 and $Ti_3C_2T_2$ MXenes have also been investigated by the new method, and no negative frequency in the whole first Brillouin zone indicates that all these terminated Ti_2CT_2 and $Ti_3C_2T_2$ MXenes (T = O, F, and OH) are dynamically stable (Figures S9 and S10), in agreement with our earlier work.[54,55]

Here we focus on Nb_2CT_2 and $Nb_4C_3T_2$ MXenes. Unlike the situation in Ti−C systems, however, not all functionalized members in Nb-containing MXenes are dynamically stable. Though bare Nb_2C and Nb_4C_3 and functionalized $Nb_4C_3O_2$, $Nb_3C_3F_2$, $Nb_4C_3(OH)_2$, and Nb_2CO_2 are dynamically stable (Figure S11), the ground-state *Cm* Nb_2CF_2 and *P*3*m*1 $Nb_2C(OH)_2$ MXenes are dynamically unstable. As shown in Figure S12, the soft modes cross the whole range of the Brillouin zone, possibly pointing to a continuous range of wavelengths at which *Cm* Nb_2CF_2 and *P*3*m*1 $Nb_2C(OH)_2$ are unstable.[56,57] Note that the searched *Cm* Nb_2CF_2 and *P*3*m*1 $Nb_2C(OH)_2$ are displacive phases; therefore, we also investigated phonon dispersions of nondisplacive $P\bar{3}m1$ Nb_2CF_2 and $Nb_2C(OH)_2$. For $P\bar{3}m1$ Nb_2CF_2 and $Nb_2C(OH)_2$, only some imaginary frequencies of ZA occur. To exclude the possible reasons arose from improper treatment of interatomic potentials containing 4d electrons, we also employed the GGA + U (U = 6.5 eV[34]) method for $P\bar{3}m1$ Nb_2CF_2 and $Nb_2C(OH)_2$, but there was no improvement, as shown in Figure S12e,f. Frozen-phonon calculations[58] were further performed to track the atomic movement associated with the soft phonon modes of $P\bar{3}m1$ Nb_2CF_2 and $Nb_2C(OH)_2$. The total energy for a series of atomic displacements along the vibration direction of the soft ZA mode was calculated and presented in Figures S13 and S14. The instability of $P\bar{3}m1$ Nb_2CF_2 and $Nb_2C(OH)_2$ is evidenced by the double-well potential. It is noteworthy that the subsequent optimization of the nearest minimum results in new structures which show an obvious displacive tendency toward the as-searched *Cm* Nb_2CF_2 and *P*3*m*1 $Nb_2C(OH)_2$. So far, both the nondisplacive and displacive Nb_2CF_2 and $Nb_2C(OH)_2$ have been demonstrated dynamically unstable. This work, along with the previous reports,[48,59] indicates that not all kinds of terminated MXenes are subject to experimental synthesis.

Micro-Raman spectroscopy is a powerful tool in the detection surface structure due to its bond-specific sensitivity

DOI: 10.1021/acs.jpcc.8b04427
J. Phys. Chem. C 2018, 122, 18501−18509

and high resolution of vibrational energy. In most Raman spectroscopy studies of MXenes, experimental data are easily available, but an adequate interpretation of the observed bands has been lacking.[6,8,60] Based on our systematic study of Raman spectra of MXenes, the Raman-active modes of MXenes can be cataloged into high-frequency internal modes and low-frequency external modes of *M*-centered polyhedra (full details are provided in Figures S15−S18). Figure 6 shows the calculated Raman shifts and experimentally collected spectra of four kinds of MXenes studied above. The Raman spectra of $Ti_3C_2T_x$ and Ti_2CT_x can be well assigned according to the calculated Raman shift, in good agreement with our earlier work.[54,55] Though there are more peaks in the spectra of $Nb_4C_3T_x$, under the guidance of the calculated Raman shifts, most peaks can still be well assigned. In Nb_2CT_x MXenes, Raman shifts of Nb_2C and Nb_2CO_2 can explain most peaks in the Raman spectrum. This is in agreement with the theoretical prediction that Nb_2C and Nb_2CO_2 are dynamically stable while Nb_2CF_2 and $Nb_2C(OH)_2$ are not. Because of the easy oxidation nature of MXenes,[46,61] some peaks of B−Nb_2O_5 are also detected together with those of MXenes (the band at 765 cm^{-1} probably corresponds to B−Nb_2O_5[62]). Besides, the oxygen-predominant functional groups presumably enable Nb_2CT_x superior lithium capacity over their counterpart Ti_2CT_x though the latter has a higher theoretical specific capacity.[63−65]

Then one question arises: can the calculated Raman shifts based on the homogeneously terminated model reasonably explain the experimental Raman spectra of multicomponent MXenes? Although further studies are required to clarify this question, a possible tentative explanation is provided here. As a precise microstructure detective method, micro-Raman spectroscopy has been demonstrated to be an effective method to probe the local structure information at the molecular level, even in many disorder/short-range-order systems such as the amorphous covalent solid.[66] Numerous Raman spectroscopy studies of molecular glasses, amorphous silicon, and carbon indicate that the Raman scattering information reflects short-range ordering.[67−69] This is also true for nonperiodic molecules as evidenced by the fact that carbon nanotubes with different diameters have similar D and G modes (the underlying physics is the local structure of C−C sp^2 hybridization they all share).[70] According to the above surface structure survey, the intact adsorption sites upon the varied termination components indicate that the functionalized MXene structure exhibits topological order. The topologically ordered structure is mosaic of homogeneously terminated MXenes with local order reserved.[46] These short-order local molecular vibrations are reflected by Raman spectra; thus, the Raman-active frequencies calculated by the homogeneously terminated model can be used to analyze the experimental spectra. On the other hand, due to the breaking of symmetry from long-range order, extra vibration modes are activated, and the spectra of MXenes show a broad feature, as shown in Figure 6.

CONCLUSIONS

In summary, we have presented a prototype of stable surface structure prediction in four typical functionalized MXenes by high-throughput computation. The ground-state configurations of these four functionalized MXenes are successfully pointed out. The distribution of functional groups shows a feature of maximizing the mixing degree at a given component as evidenced by the repulsive interaction between identical species. The main factors contribute to the free energy follow the order: termination species > adsorption sites > in-plane distribution pattern > the interaction of terminations distribution pattern on each side of one layer. Oxygen-terminated MXenes are the most stable while OH-terminated MXenes have a tendency to transform to O-terminated MXenes and H_2 gas. Moreover, Nb_2CF_2 and $Nb_2C(OH)_2$ are dynamically unstable due to competing displacive phases. The predicted surface structures of MXenes via high-throughput computation combining with the lattice dynamics calculations are verified by micro-Raman spectroscopy. The methodology and results presented in this work are of guiding significance to the rational design of the big family of MXenes and are applicable to other relevant termination-functionalized 2D materials as well.

ASSOCIATED CONTENT

Supporting Information

The Supporting Information is available free of charge on the ACS Publications website at DOI: 10.1021/acs.jpcc.8b04427.

Additional details about structure screening; phonon calculation; assignment of Raman-active vibration modes; and ground-state crystal structures of multi-component MXenes (PDF)

AUTHOR INFORMATION

Corresponding Authors

*(X.W.) E-mail: wang@imr.ac.cn.
*(W.L.) E-mail: wu.li@szu.edu.cn.

ORCID

Xiaohui Wang: 0000-0001-7271-2662

Notes

The authors declare no competing financial interest.

ACKNOWLEDGMENTS

This work was supported by the Youth Innovation Promotion Association, Chinese Academy of Sciences (CAS), under Grant No. 2011152, and Shenyang National Laboratory for Materials Science, Institute of Metal Research, CAS under Grant No. 2017RP06, and Special Program for Applied Research on Super Computation of the NSFC-Guangdong Joint Fund (the second phase) under Grant No. U1501501.

REFERENCES

(1) Ma, Z.; Zaera, F. Competitive Chemisorption between Pairs of Cinchona Alkaloids and Related Compounds from Solution onto Platinum Surfaces. *J. Am. Chem. Soc.* **2006**, *128*, 16414−16415.

(2) Morin, C.; Simon, D.; Sautet, P. Trends in the Chemisorption of Aromatic Molecules on a Pt(111) Surface: Benzene, Naphthalene, and Anthracene from First Principles Calculations. *J. Phys. Chem. B* **2004**, *108*, 12084−12091.

(3) Soriaga, M. P.; Song, D.; Zapien, D. C.; Hubbard, A. T. Competitive Chemisorption from Binary Surfactant Mixtures at Solid Liquid Interfaces-Hydroquinone and Naphthohydroquinone at Smooth Polycrystalline Platinum in Aqueous-Solutions. *Langmuir* **1985**, *1*, 123−127.

(4) Abild-Pedersen, F.; Greeley, J.; Studt, F.; Rossmeisl, J.; Munter, T. R.; Moses, P. G.; Skulason, E.; Bligaard, T.; Norskov, J. K. Scaling Properties of Adsorption Energies for Hydrogen-Containing Molecules on Transition-Metal Surfaces. *Phys. Rev. Lett.* **2007**, *99*, 016105.

DOI: 10.1021/acs.jpcc.8b04427
J. Phys. Chem. C 2018, 122, 18501−18509

(5) Parsons, D. F.; Salis, A. The Impact of the Competitive Adsorption of Ions at Surface Sites on Surface Free Energies and Surface Forces. *J. Chem. Phys.* **2015**, *142*, 134707.
(6) Naguib, M.; Kurtoglu, M.; Presser, V.; Lu, J.; Niu, J. J.; Heon, M.; Hultman, L.; Gogotsi, Y.; Barsoum, M. W. Two-Dimensional Nanocrystals Produced by Exfoliation of Ti_3AlC_2. *Adv. Mater.* **2011**, *23*, 4248−4253.
(7) Naguib, M.; Mashtalir, O.; Carle, J.; Presser, V.; Lu, J.; Hultman, L.; Gogotsi, Y.; Barsoum, M. W. Two-Dimensional Transition Metal Carbides. *ACS Nano* **2012**, *6*, 1322−1331.
(8) Naguib, M.; Mochalin, V. N.; Barsoum, M. W.; Gogotsi, Y. 25th Anniversary Article: MXenes: A New Family of Two-Dimensional Materials. *Adv. Mater.* **2014**, *26*, 992−1005.
(9) Anasori, B.; Lukatskaya, M. R.; Gogotsi, Y. 2D Metal Carbides and Nitrides (MXenes) for Energy Storage. *Nat. Rev. Mater.* **2017**, *2*, 16098.
(10) Shahzad, F.; Alhabeb, M.; Hatter, C. B.; Anasori, B.; Man Hong, S.; Koo, C. M.; Gogotsi, Y. Electromagnetic Interference Shielding with 2D Transition Metal Carbides (MXenes). *Science* **2016**, *353*, 1137−1140.
(11) Ghidiu, M.; Lukatskaya, M. R.; Zhao, M. Q.; Gogotsi, Y.; Barsoum, M. W. Conductive Two-Dimensional Titanium Carbide 'Clay' with High Volumetric Capacitance. *Nature* **2014**, *516*, 78−81.
(12) Hu, M. M.; Li, Z. J.; Hu, T.; Zhu, S. H.; Zhang, C.; Wang, X. H. High-Capacitance Mechanism for $Ti_3C_2T_x$ MXene by in Situ Electrochemical Raman Spectroscopy Investigation. *ACS Nano* **2016**, *10*, 11344−11350.
(13) Tang, Q.; Zhou, Z.; Shen, P. W. Are MXenes Promising Anode Materials for Li Ion Batteries? Computational Studies on Electronic Properties and Li Storage Capability of Ti_3C_2 and $Ti_3C_2X_2$ (X = F, OH) Monolayer. *J. Am. Chem. Soc.* **2012**, *134*, 16909−16916.
(14) Peng, Q. M.; Guo, J. X.; Zhang, Q. R.; Xiang, J. Y.; Liu, B. Z.; Zhou, A. G.; Liu, R. P.; Tian, Y. J. Unique Lead Adsorption Behavior of Activated Hydroxyl Group in Two-Dimensional Titanium Carbide. *J. Am. Chem. Soc.* **2014**, *136*, 4113−4116.
(15) Kumar, H.; Frey, N. C.; Dong, L.; Anasori, B.; Gogotsi, Y.; Shenoy, V. B. Tunable Magnetism and Transport Properties in Nitride MXenes. *ACS Nano* **2017**, *11*, 7648−7655.
(16) Li, N.; Chen, X.; Ong, W. J.; MacFarlane, D. R.; Zhao, X.; Cheetham, A. K.; Sun, C. Understanding of Electrochemical Mechanisms for CO_2 Capture and Conversion into Hydrocarbon Fuels in Transition-Metal Carbides (MXenes). *ACS Nano* **2017**, *11*, 10825−10833.
(17) Kim, S. J.; et al. Metallic $Ti_3C_2T_x$ MXene Gas Sensors with Ultrahigh Signal-to-Noise Ratio. *ACS Nano* **2018**, *12*, 986−993.
(18) Okubo, M.; Sugahara, A.; Kajiyama, S.; Yamada, A. MXene as a Charge Storage Host. *Acc. Chem. Res.* **2018**, *51*, 591−599.
(19) Hu, T.; Li, Z. J.; Hu, M. M.; Wang, J. M.; Hu, Q. M.; Li, Q. Z.; Wang, X. H. Chemical Origin of Termination-Functionalized MXenes: $Ti_3C_2T_2$ as a Case Study. *J. Phys. Chem. C* **2017**, *121*, 19254−19261.
(20) Khazaei, M.; Ranjbar, A.; Arai, M.; Sasaki, T.; Yunoki, S. Electronic Properties and Applications of MXenes: A Theoretical Review. *J. Mater. Chem. C* **2017**, *5*, 2488−2503.
(21) Yang, J.-H.; Zhang, S.-Z.; Ji, J.-L.; Wei, S.-H. Adsorption Activities of O, OH, F and Au on Two-Dimensional Ti_2C and Ti_3C_2 Surfaces. *Acta Phys.-Chim. Sin.* **2015**, *31*, 369−376.
(22) Hope, M. A.; Forse, A. C.; Griffith, K. J.; Lukatskaya, M. R.; Ghidiu, M.; Gogotsi, Y.; Grey, C. P. NMR Reveals the Surface Functionalisation of Ti_3C_2 MXene. *Phys. Chem. Chem. Phys.* **2016**, *18*, 5099−102.
(23) Wang, H.-W.; Naguib, M.; Page, K.; Wesolowski, D. J.; Gogotsi, Y. Resolving the Structure of $Ti_3C_2T_x$ MXenes through Multilevel Structural Modeling of the Atomic Pair Distribution Function. *Chem. Mater.* **2016**, *28*, 349−359.
(24) Magne, D.; Mauchamp, V.; Celerier, S.; Chartier, P.; Cabioc'h, T. Site-Projected Electronic Structure of Two-Dimensional Ti_3C_2 MXene: The Role of the Surface Functionalization Groups. *Phys. Chem. Chem. Phys.* **2016**, *18*, 30946−30953.
(25) Halim, J.; Cook, K. M.; Naguib, M.; Eklund, P.; Gogotsi, Y.; Rosen, J.; Barsoum, M. W. X-Ray Photoelectron Spectroscopy of Select Multi-Layered Transition Metal Carbides (MXenes). *Appl. Surf. Sci.* **2016**, *362*, 406−417.
(26) Champagne, A.; Shi, L.; Ouisse, T.; Hackens, B.; Charlier, J.-C. Electronic and Vibrational Properties of V_2C-Based MXenes: From Experiments to First-Principles Modeling. *Phys. Rev. B: Condens. Matter Mater. Phys.* **2018**, *97*, 115439.
(27) Tan, T. L.; Jin, H. M.; Sullivan, M. B.; Anasori, B.; Gogotsi, Y. High-Throughput Survey of Ordering Configurations in MXene Alloys across Compositions and Temperatures. *ACS Nano* **2017**, *11*, 4407−4418.
(28) Wang, Y.; Lv, J.; Zhu, L.; Ma, Y. Calypso: A Method for Crystal Structure Prediction. *Comput. Phys. Commun.* **2012**, *183*, 2063−2070.
(29) Gao, B.; Shao, X.; Lv, J.; Wang, Y.; Ma, Y. Structure Prediction of Atoms Adsorbed on Two-Dimensional Layer Materials: Method and Applications. *J. Phys. Chem. C* **2015**, *119*, 20111−20118.
(30) Kresse, G.; Furthmuller, J. Efficient Iterative Schemes for Ab Initio Total-Energy Calculations Using a Plane-Wave Basis Set. *Phys. Rev. B: Condens. Matter Mater. Phys.* **1996**, *54*, 11169−11186.
(31) Blöchl, P. E. Projector Augmented-Wave Method. *Phys. Rev. B: Condens. Matter Mater. Phys.* **1994**, *50*, 17953−17979.
(32) Perdew, J. P.; Burke, K.; Ernzerhof, M. Generalized Gradient Approximation Made Simple. *Phys. Rev. Lett.* **1996**, *77*, 3865−3868.
(33) Zhao, S.; Kang, W.; Xue, J. Manipulation of Electronic and Magnetic Properties of M_2C (M = Hf, Nb, Sc, Ta, Ti, V, Zr) Monolayer by Applying Mechanical Strains. *Appl. Phys. Lett.* **2014**, *104*, 133106.
(34) Hu, J.; Xu, B.; Ouyang, C.; Zhang, Y.; Yang, S. A. Investigations on Nb_2C Monolayer as Promising Anode Material for Li or Non-Li Ion Batteries from First-Principles Calculations. *RSC Adv.* **2016**, *6*, 27467−27474.
(35) Khazaei, M.; Arai, M.; Sasaki, T.; Chung, C.-Y.; Venkataramanan, N. S.; Estili, M.; Sakka, Y.; Kawazoe, Y. Novel Electronic and Magnetic Properties of Two-Dimensional Transition Metal Carbides and Nitrides. *Adv. Funct. Mater.* **2013**, *23*, 2185−2192.
(36) Gandi, A. N.; Alshareef, H. N.; Schwingenschlögl, U. Thermoelectric Performance of the MXenes M_2CO_2 (M = Ti, Zr, or Hf). *Chem. Mater.* **2016**, *28*, 1647−1652.
(37) Gao, G.; O'Mullane, A. P.; Du, A. 2D MXenes: A New Family of Promising Catalysts for the Hydrogen Evolution Reaction. *ACS Catal.* **2017**, *7*, 494−500.
(38) Togo, A.; Tanaka, I. First Principles Phonon Calculations in Materials Science. *Scr. Mater.* **2015**, *108*, 1−5.
(39) Wang, X. H.; Zhou, Y. C. Solid−Liquid Reaction Synthesis of Layered Machinable Ti_3AlC_2 Ceramic. *J. Mater. Chem.* **2002**, *12*, 455−460.
(40) Zhang, H.; Hu, T.; Wang, X. H.; Li, Z. J.; Hu, M. M.; Wu, E. D.; Zhou, Y. C. Discovery of Carbon-Vacancy Ordering in Nb_4AlC_{3-x} under the Guidance of First-Principles Calculations. *Sci. Rep.* **2015**, *5*, 14192.
(41) Wang, X. H.; Zhou, Y. C. Solid-Liquid Reaction Synthesis and Simultaneous Densification of Polycrystalline Ti_2AlC. *Z. Metallkd.* **2002**, *93*, 66−71.
(42) Hu, C.; Li, F.; Zhang, J.; Wang, J.; Wang, J.; Zhou, Y. Nb_4AlC_3: A New Compound Belonging to the MAX Phases. *Scr. Mater.* **2007**, *57*, 893−896.
(43) Seh, Z. W.; Fredrickson, K. D.; Anasori, B.; Kibsgaard, J.; Strickler, A. L.; Lukatskaya, M. R.; Gogotsi, Y.; Jaramillo, T. F.; Vojvodic, A. Two-Dimensional Molybdenum Carbide (MXene) as an Efficient Electrocatalyst for Hydrogen Evolution. *ACS Energy Lett.* **2016**, *1*, 589−594.
(44) Pandey, M.; Thygesen, K. S. Two-Dimensional MXenes as Catalysts for Electrochemical Hydrogen Evolution: A Computational Screening Study. *J. Phys. Chem. C* **2017**, *121*, 13593−13598.
(45) Karlsson, L. H.; Birch, J.; Halim, J.; Barsoum, M. W.; Persson, P. O. Atomically Resolved Structural and Chemical Investigation of Single MXene Sheets. *Nano Lett.* **2015**, *15*, 4955−4960.

DOI: 10.1021/acs.jpcc.8b04427
J. Phys. Chem. C 2018, 122, 18501−18509

(46) Palisaitis, J.; Persson, I.; Halim, J.; Rosen, J.; Persson, P. O. A. On the Structural Stability of MXene and the Role of Transition Metal Adatoms. *Nanoscale* **2018**, *10*, 10850−10855.
(47) Ashton, M.; Mathew, K.; Hennig, R. G.; Sinnott, S. B. Predicted Surface Composition and Thermodynamic Stability of MXenes in Solution. *J. Phys. Chem. C* **2016**, *120*, 3550−3556.
(48) Yorulmaz, U.; Ozden, A.; Perkgoz, N. K.; Ay, F.; Sevik, C. Vibrational and Mechanical Properties of Single Layer MXene Structures: A First-Principles Investigation. *Nanotechnology* **2016**, *27*, 335702.
(49) Mishra, A.; Srivastava, P.; Carreras, A.; Tanaka, I.; Mizuseki, H.; Lee, K.-R.; Singh, A. K. Atomistic Origin of Phase Stability in Oxygen-Functionalized MXene: A Comparative Study. *J. Phys. Chem. C* **2017**, *121*, 18947−18953.
(50) Umrigar, C.; Ellis, D. E. Embedded Cluster Model of NbO_2: Compton Profile and Electronic Spectra. *Phys. Rev. B: Condens. Matter Mater. Phys.* **1980**, *21*, 852−861.
(51) Yang, X.-F.; Wang, A.; Qiao, B.; Li, J.; Liu, J.; Zhang, T. Single-Atom Catalysts: A New Frontier in Heterogeneous Catalysis. *Acc. Chem. Res.* **2013**, *46*, 1740−1748.
(52) Lukatskaya, M. R.; et al. Ultra-High-Rate Pseudocapacitive Energy Storage in Two-Dimensional Transition Metal Carbides. *Nature Energy* **2017**, *2*, 17105.
(53) Carrete, J.; Li, W.; Lindsay, L.; Broido, D. A.; Gallego, L. J.; Mingo, N. Physically Founded Phonon Dispersions of Few-Layer Materials and the Case of Borophene. *Mater. Res. Lett.* **2016**, *4*, 204−211.
(54) Hu, T.; Wang, J. M.; Zhang, H.; Li, Z. J.; Hu, M. M.; Wang, X. H. Vibrational Properties of Ti_3C_2 and $Ti_3C_2T_2$ (T = O, F, OH) Monosheets by First-Principles Calculations: A Comparative Study. *Phys. Chem. Chem. Phys.* **2015**, *17*, 9997−10003.
(55) Hu, T.; Hu, M. M.; Li, Z. J.; Zhang, H.; Zhang, C.; Wang, J. M.; Wang, X. H. Covalency-Dependent Vibrational Dynamics in Two-Dimensional Titanium Carbides. *J. Phys. Chem. A* **2015**, *119*, 12977−12984.
(56) Skelton, J. M.; et al. Anharmonicity in the High-Temperature *Cmcm* Phase of SnSe: Soft Modes and Three-Phonon Interactions. *Phys. Rev. Lett.* **2016**, *117*, 075502.
(57) da Silva, E. L.; Skelton, J. M.; Parker, S. C.; Walsh, A. Phase Stability and Transformations in the Halide Perovskite $CsSnI_3$. *Phys. Rev. B: Condens. Matter Mater. Phys.* **2015**, *91*, 144107.
(58) Li, Q.; Zhou, D.; Zheng, W.; Ma, Y.; Chen, C. Global Structural Optimization of Tungsten Borides. *Phys. Rev. Lett.* **2013**, *110*, 136403.
(59) Lei, J.; Kutana, A.; Yakobson, B. I. Predicting Stable Phase Monolayer Mo_2C (MXene), a Superconductor with Chemically-Tunable Critical Temperature. *J. Mater. Chem. C* **2017**, *5*, 3438−3444.
(60) Soundiraraju, B.; George, B. K. Two-Dimensional Titanium Nitride (Ti_2N) MXene: Synthesis, Characterization, and Potential Application as Surface-Enhanced Raman Scattering Substrate. *ACS Nano* **2017**, *11*, 8892−8900.
(61) Zhang, C. J.; et al. Oxidation Stability of Colloidal Two-Dimensional Titanium Carbides (MXenes). *Chem. Mater.* **2017**, *29*, 4848−4856.
(62) Nico, C.; Soares, M. R. N.; Rodrigues, J.; Matos, M.; Monteiro, R.; Graça, M. P. F.; Valente, M. A.; Costa, F. M.; Monteiro, T. Sintered NbO Powders for Electronic Device Applications. *J. Phys. Chem. C* **2011**, *115*, 4879−4886.
(63) Mashtalir, O.; Lukatskaya, M. R.; Zhao, M. Q.; Barsoum, M. W.; Gogotsi, Y. Amine-Assisted Delamination of Nb_2C MXene for Li-Ion Energy Storage Devices. *Adv. Mater.* **2015**, *27*, 3501.
(64) Naguib, M.; Halim, J.; Lu, J.; Cook, K. M.; Hultman, L.; Gogotsi, Y.; Barsoum, M. W. New Two-Dimensional Niobium and Vanadium Carbides as Promising Materials for Li-Ion Batteries. *J. Am. Chem. Soc.* **2013**, *135*, 15966−15969.
(65) Xie, Y.; Naguib, M.; Mochalin, V. N.; Barsoum, M. W.; Gogotsi, Y.; Yu, X. Q.; Nam, K. W.; Yang, X. Q.; Kolesnikov, A. I.; Kent, P. R. Role of Surface Structure on Li-Ion Energy Storage Capacity of Two-Dimensional Transition-Metal Carbides. *J. Am. Chem. Soc.* **2014**, *136*, 6385−6394.
(66) Chehaidar, A.; Zwick, A.; Carles, R.; Bandet, J. Multiple-Order Raman Scattering and the Density of Vibrational States in α-GaAs. *Phys. Rev. B: Condens. Matter Mater. Phys.* **1994**, *50*, 5345−5351.
(67) Brawer, S. Theory of the Vibrational Spectra of Some Network and Molecular Glasses. *Phys. Rev. B* **1975**, *11*, 3173−3194.
(68) Smith, J. E.; Brodsky, M. H.; Crowder, B. L.; Nathan, M. I.; Pinczuk, A. Raman Spectra of Amorphous Si and Related Tetrahedrally Bonded Semiconductors. *Phys. Rev. Lett.* **1971**, *26*, 642−646.
(69) Yndurain, F. Vibrational Properties of Alloys: Study of Si_xGe_{1-x}. *Phys. Rev. B: Condens. Matter Mater. Phys.* **1978**, *18*, 2876−2883.
(70) Kakihana, M.; Osada, M. Raman Spectroscopy as a Characterization Tool for Carbon Materials. *Carbon Alloys* **2003**, 285−298.

DOI: 10.1021/acs.jpcc.8b04427
J. Phys. Chem. C 2018, 122, 18501−18509